

# A Spectrum-Adaptive Decomposition Method for Effective Atomic Number Estimation Using Dual Energy CT

Ankit Manerikar, Fangda Li, Avinash C. Kak; School of Electrical and Computer Engineering, Purdue University; West Lafayette, Indiana, USA.

## Abstract

*Dual Energy Computed Tomography (DECT) is expected to become a significant tool for voxel-based detection of hazardous materials in airport baggage screening. The traditional approach to DECT imaging involves collecting the projection data using two different X-ray spectra and then decomposing the data thus collected into line integrals of two independent characterizations of the material properties. Typically, one of these characterizations involves the effective atomic number ( $Z_{eff}$ ) of the materials. However, with the X-ray spectral energies typically used for DECT imaging, the current best-practice approaches for dual-energy decomposition yield  $Z_{eff}$  values whose accuracy range is limited to only a subset of the periodic-table elements, more specifically to ( $Z < 30$ ). Although this estimation can be improved by using a system-independent  $\rho_e - Z_e$  (SIRZ) space, the SIRZ transformation does not efficiently model the polychromatic nature of the X-ray spectra typically used in physical CT scanners. In this paper, we present a new decomposition method, AdaSIRZ, that corrects this shortcoming by adapting the SIRZ decomposition to the entire spectrum of an X-ray source. The method reformulates the X-ray attenuation equations as direct functions of ( $\rho_e, Z_e$ ) and solves for the coefficients using bounded nonlinear least-squares optimization. Performance comparison of AdaSIRZ with other  $Z_{eff}$  estimation methods on different sets of real DECT images shows that AdaSIRZ provides a higher output accuracy for  $Z_{eff}$  image reconstructions for a wider range of object materials.*

## Introduction

Material characterization using Dual Energy Computed Tomography (DECT) is expected to play an important role in security screening for the detection of threat materials as it leads directly to a voxel-level determination of the chemical composition of the contents of a baggage. DECT involves simultaneously scanning an object volume using two different X-ray spectra and decomposing the projection data collected into line integrals of the parameters that can be used to characterize the chemical composition of each voxel. One such parameter is the effective atomic number ( $Z_{eff}$ ) [1] — a parameter that is important for identifying hazardous material signatures. The methods described in this paper are expected to improve the estimation of  $Z_{eff}$  for baggage inspection using DECT projection data in security scanners.

Typically, the dual-energy projection data is decomposed into Compton and Photoelectric (PE) co-efficient line integrals, which is then followed by a voxel-wise calculation of  $Z_{eff}$  from the reconstructed Compton and PE images. The underlying math-

ematical formulation for this decomposition [2] models X-ray projections as linear combinations of energy dependent basis functions representing the Compton and PE effects. This linear approximation, however, does not account for higher-order discontinuities in the X-ray absorption spectra, which bounds the accuracy of  $Z_{eff}$  estimation to a subset of the natural elements. Considering the high variability of the objects typically found in a scanned bag, this limits the extent to which material characterization can be performed with this method.

Recent studies in  $Z_{eff}$  estimation have resulted in several modifications to the traditional DECT model based on the estimation of the Compton and PE line integrals in the projection data. The most significant of these modifications projects the parameters reconstructed from the dual-energy projection data into a system-independent  $\rho_e - Z_e$  (SIRZ) space [3] by taking advantage of the fact that the X-ray attenuation depends directly on  $Z_{eff}$ . The new method, however, calculates the DECT parameters by approximating the X-ray source as a monochromatic spectrum, an assumption that does not reflect the nature of practical X-ray sources in physical CT scanners [4].

In this paper, we propose a modified decomposition method that extends the Monochromatic SIRZ decomposition of [4] to the entire spectrum of an X-ray source. The proposed Adaptive SIRZ (AdaSIRZ) method reformulates the X-ray attenuation equations as direct functions of ( $Z_e, \rho_e$ ) and solves for their values using bounded nonlinear least-squares optimization. Here, the polychromatic X-ray spectra are incorporated into the forward model while computing the optimization residuals. We have tested the AdaSIRZ method for its performance on simulated as well as real DECT images in the ALERT TO-3 dataset [5] and compared it with the existing methods for  $Z_{eff}$  estimation. The performance comparison shows that AdaSIRZ provides accurate atomic number estimations for a wider range of natural elements.

The paper is organized as follows: (i) Section II provides a literary survey of  $Z_{eff}$  estimation methods, (ii) Section III gives an overview on DECT operation, the limits on  $Z_{eff}$  estimation and SIRZ decomposition, (iii) Section IV elaborates on the proposed Adaptive SIRZ decomposition method, and (iv) finally, Section V enumerates the performance results for AdaSIRZ on simulated images and the ALERT TO-3 dataset [5].

## Related Work

This section presents an overview of the relevant research in DECT and on  $Z_{eff}$  estimation methods for threat detection. Several of these works will be revisited in the upcoming sections for the mathematical formulation of the proposed AdaSIRZ method.

The effective atomic number,  $Z_{eff}$ , which represents the av-

This research was funded by the BAA 17-03 AATR contract with Department of Homeland Security's Science and Technology Directorate.

erage atomic number of a compound/mixture, has proved useful for estimating the chemical composition from radiological interactions since 1965 [1]. The seminal paper on DECT by Alvarez and Macovski [6] was one of the first to present the correlation between X-ray attenuation and  $Z_{eff}$  by formulating the DECT Compton and PE coefficients as functions of  $Z_{eff}$ . As to how these  $Z_{eff}$ -based relationships could be exploited for identifying explosive materials was explored in [7][8]. Subsequently, in 2004, Ying et al. [2] used the same relationships to present a computational framework for Dual Energy CT for explosives detection. That paper describes a constrained decomposition method (CDM) which decomposes a pair of DE projection values using bounded optimization and estimates the Compton and PE line integrals for calculating the  $Z_{eff}$  values. There are variants to this method that improve the operation by using optimization tools such as those presented [9] [10], but the attenuation model for all these methods derives  $Z_{eff}$  estimates from the Compton and PE line integrals.

In this paper, we first discuss the limits on the atomic number  $Z$  within which the estimated  $Z_{eff}$  values can be trusted for a given spectral model. We then describe how the CDM method for projection-data decomposition can be improved through parametrization into a system-independent  $\rho_e - Z_e$  (SIRZ) space. The SIRZ decomposition model was first proposed in [3] to provide a scanner-agnostic subspace for material characterization using Dual Energy CT. This required formulating the dual-energy x-ray attenuation in terms of the electron density  $\rho_e$  and  $Z_{eff}$ . This alternative DECT parameter space was also suggested in [11].

A recent variant of the SIRZ method [4] improves the  $\rho_e - Z_e$  estimation by using material basis functions and spectral calibration. However, since this method is based on the monochromatic assumption for the X-ray sources, the estimated  $Z_{eff}$  values must be adjusted empirically for them to be useful for downstream calculations. In this paper, we propose a new version of the SIRZ decomposition method, the Adaptive SIRZ (AdaSIRZ), that adapts the monochromatic SIRZ decomposition to the entire X-ray spectrum. The mathematical background for the AdaSIRZ model and its implementation are described in the next section of the paper.

## System Overview

This section presents the mathematical preliminaries for using Dual Energy CT for material detection. This includes a brief overview of the DECT attenuation model,  $Z_{eff}$  estimation and its operating limits, and the monochromatic SIRZ method.

### Dual Energy CT — Theory of Operation

Extracting material-specific properties with DECT is based on exploiting the energy dependence of X-ray attenuation in the CT images constructed with different spectra [6]. For a single X-ray projection, the attenuation equation takes the following form:

$$P = -\ln \left[ \int S(E) \cdot e^{-\int \mu(l,E) dl} \cdot dE \right] + S_0 \quad (1)$$

where  $P$  denotes the X-ray projection,  $S(E)$  is the source spectral distribution,  $\mu(l,E)$  is the linear attenuation coefficient along the path  $l$  and  $S_0$  is the flat-field correction. It is common to express the energy dependence of the X-ray attenuation  $\mu(l,E)$  in Eq. (1) as a linear sum of two energy dependent basis functions, one de-

rived from the Compton effect and the other from PE effect:

$$\mu(l,E) = a_c(l) \cdot f_{KN}(E) + a_p(l) \cdot f_p(E) \quad (2)$$

where  $a_p(l)$  and  $a_c(l)$  denote the PE and Compton coefficients specific to the material at  $l \equiv (x,y,z)$  and where  $f_{KN}(E)$  and  $f_p(E)$  are the PE and Compton basis functions given by:

$$\begin{aligned} f_p(E) &= (1/E)^3 \\ f_{KN}(E) &= \frac{1+\alpha}{\alpha^2} \left[ \frac{2(1+\alpha)}{1+2\alpha} - \frac{1}{\alpha} \ln\{1+2\alpha\} \right] \\ &\quad + \frac{1}{2\alpha} \ln\{1+2\alpha\} - \frac{1+3\alpha}{(1+2\alpha)^2} \end{aligned} \quad (3)$$

where  $\alpha = (E/510.975 \text{ KeV})$ . With this formulation, DECT X-ray projections obtained for two different X-ray spectra  $S_1(E)$  and  $S_2(E)$  can be expressed as:

$$P_1 = -\ln \left[ \int S_1(E) \cdot e^{\{-A_p \cdot f_p(E) - A_c \cdot f_{KN}(E)\}} \cdot dE \right] + S_{1,0} \quad (4)$$

$$P_2 = -\ln \left[ \int S_2(E) \cdot e^{\{-A_p \cdot f_p(E) - A_c \cdot f_{KN}(E)\}} \cdot dE \right] + S_{2,0} \quad (5)$$

where  $A_p = \int a_p(l) \cdot dl$ ,  $A_c = \int a_c(l) \cdot dl$ . That is,  $A_p, A_c$ , are the line integrals of the PE and Compton coefficients,  $a_p, a_c$  respectively. Since the spectral distributions  $S_1(E)$  and  $S_2(E)$  can be determined beforehand, Eqs. (4) and (5) can be solved for the measured projections  $\bar{P}_1, \bar{P}_2$  as a non-linear least squares optimization problem as shown below [2]:

$$A_c^*, A_p^* = \underset{A_c, A_p}{\operatorname{argmin}} \sum_{i \in \{1,2\}} [P_i(A_c, A_p) - \bar{P}_i]^2 \quad (6)$$

### Effective Atomic Number $Z_{eff}$ and its Estimation

The effective atomic number  $Z_{eff}$  is a commonly used property for estimating chemical composition of a material through X-ray interactions. Here is a classic definition of  $Z_{eff}$  from [12]:

$$Z_{eff} = \sqrt[p]{\sum_{i=1}^N w_i Z_i^p}, \quad \text{where } w_i = \frac{n_i Z_i}{\sum_{j=1}^N n_j Z_j} \quad (7)$$

Here  $p$  is an empirical constant generally set to 2.94,  $N$  is the number of constituent elements in the material and  $Z_i$  is the atomic number of the  $i^{th}$  element with  $w_i$  being its relative electron fraction and  $n_i$  the number of units of  $Z_i$  within the material. Alvarez and Macovski use this definition of  $Z_{eff}$  to express the PE and the Compton coefficients [6] as follows:

$$a_p \approx K_1 \frac{\rho_e}{A} Z_{eff}^n; \quad a_c \approx K_2 \frac{\rho_e}{A} Z_{eff} \quad (8)$$

where  $\rho_e$  is the electron density, the exponent  $n$  a constant whose value is approximately between 3.5 and 4.5 and  $A$  a constant related to the detector aperture. The two equations shown above straightforwardly yield the following expression for  $Z_{eff}$ :

$$Z_{eff} = K \left( \frac{a_p}{a_c} \right)^{\frac{1}{n-1}} \quad (9)$$

What this result implies is that, in order to find the value of  $Z_{eff}$  in a voxel, we first need to use a CT algorithm to construct  $a_p$  and  $a_c$  images from the decomposed line integrals shown in Eq. (6), and subsequently use the above equation to find  $Z_{eff}$ . We will refer to this approach as the baseline CPB method.

### Limits of CPB Estimation for $Z_{eff}$

The validity of the  $Z_{eff}$  estimation method described in the previous section depends strongly on the extent to which the linear approximation in Eq. (2) holds. The linear decomposition of the projection data using the Compton and PE bases does not constitute the total X-ray cross-section response for a material since Eq. (2) does not account for the higher order K- and L-edge discontinuities in the X-ray cross-sections. These discontinuities in the energy dependence of the attenuation can assume significant values for high  $Z$  elements. Additionally, the presence of the discontinuities in the energy dependence curves of the attenuation violates the differentiability of the otherwise convex optimization cost function in Eq. (6) and that can result in an unstable DE decomposition.

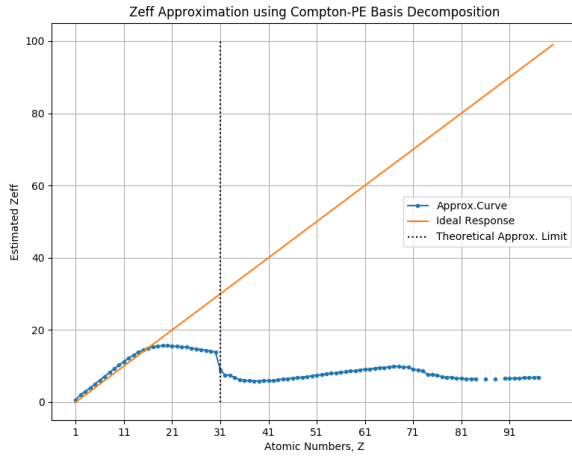


**Figure 1.**  $Z_{eff}$  approximation using Compton-PE basis decomposition for DECT. The estimated  $Z_{eff}$  values are plotted for natural elements in the range  $Z = 1$  to 100 and for source spectra with photon energies from 10 keV to 160 keV.

The consequences of the linear approximation in Eq. (6) are illustrated in Figure 1 where we have plotted the estimated  $Z_{eff}$  as produced by Eq. (9) for the range of elements from  $Z = 1$  to 100 and for the energy range from 10 keV to 160 keV. The plot was produced by using a forward model to propagate the polychromatic X-ray beam through a unit volume of pure materials that corresponds to the different atomic numbers on the horizontal axis and then using the CPD method to estimate the  $Z_{eff}$  for that material. The plot shows a gradual increase in the error between the true and the approximated values for the heavier elements with a distinct jump in the error at  $Z = 31$ . We refer to this jump as a manifestation of unstable calculation of  $Z_{eff}$ . The jump at  $Z = 31$  is for Gallium (*Ga*) and can be attributed to the presence of the K-edge discontinuities in the energy dependence of the attenuation coefficient for this material. The K absorption edge for *Ga* occurs at 10.3671 keV [13], which is just above the lower end of the energy range of 10 keV to 160 keV of the illuminating X-ray source. So, for this particular polychromatic source, *Ga* ( $Z = 31$ ) is the lightest element for which the K-edge is within the energy range (10 - 160 keV) used in our calculations. On the basis of this observation, we can now formally specify the range of elements for which the CPB decomposition can be expected to yield  $Z_{eff}$  values with reasonable accuracy:

The linear approximation for  $\mu(l, E)$  in Eq. (2) will lead to a stable dual-energy decomposition and, therefore, to a stable estimation of  $Z_{eff}$ , as long as the highest K-edge energy for the materials through which the X-ray beam is traversing is lower than the lowest energy of the incident photons in the two X-ray sources used for DECT.

This limitation in the Compton-PE basis decomposition based on the linear approximation in Eq. (2) arises from the fact that the Klein-Nishina cross-section equation (Compton basis function) in Eq. (3) does not contain the electron binding correction that would account for the K, L, and M absorption edges. The use of an alternative parameter space as shown in the next section can alleviate this error to some extent.

### The SIRZ Feature Space

The system independent  $(\rho_e, Z_e)$  (SIRZ) feature space was first introduced in [3] to provide a system-agnostic approach for DECT material characterization. The primary meaning of system dependence here is the dependence of the calculated parameters on the energy spectrum of the X-ray source.

For example, say that one wishes to use two parameters, the attenuation coefficient  $\mu$  and the effective atomic number  $Z_{eff}$ , for characterizing a material. With a mono-energetic X-ray beam, the values for both these parameters for a small sample of a material (we say “small” in order for any beam-hardening and photon starvation effects to not affect the measurements) are likely to be system independent. But, even for a small sample, that will not be the case with polyenergetic beams. So the question boils down to what parameters are least vulnerable to distortion due to the wide spectral distribution of a typical X-ray source used for imaging. The conclusion in [3] was that the electron density  $\rho_e$  and effective atomic number  $Z_{eff}$  are less vulnerable to such a distortion.

It was shown in [3] that the atomic number calculated from the X-ray attenuation measurements does not estimate exactly the  $Z_{eff}$  as a weighted combination of the elements as defined in Eq. (9). In retrospect that is not surprising since the true atomic numbers are integral values whereas any estimation based on Eq. (9) will return a floating-point value. This issue was addressed in [3] by introducing the notation  $Z_e$  to describe what is actually estimated through Eq. (9). In [3],  $Z_e$  is defined as *the fractional atomic number of a fictitious element whose cross-section (meaning attenuation) and X-ray transmission would be optimally close to that of the observed X-ray cross-sectional response in the least-squares sense.*

To elaborate, consider a fractional value for  $Z_e$  given by  $Z_e = Z' + \delta$  where  $Z' = \text{floor}(Z_e)$  is the integral part of  $Z_e$  and  $\delta$  is its fractional part. The attenuation coefficient corresponding to this  $Z_e$  is given by:

$$\sigma_e(Z_e, E) = (1 - \delta) \cdot \sigma_e(Z', E) + \delta \cdot \sigma_e(Z' + 1, E) \quad (10)$$

where  $\sigma_e(\cdot)$  denotes the electron cross-section for a natural element. With these definitions,  $Z_e$  for a given material is given by:

$$Z_e^* = \underset{Z_e}{\operatorname{argmin}} \left\{ \int S(E) \left[ e^{-M\sigma_e(Z_e, E)} - e^{-M\sigma_e(E)} \right]^2 dE \right\} \quad (11)$$

where  $S(E)$  is the X-ray spectrum,  $M$  the cumulative electron density in moles ( $e^-/\text{cm}^2$ ) and  $\sigma_e(E)$  the true attenuation response

of the material. As we shall see presently, the advantage of this interpretation for  $Z_e$  is that it is possible to have a one-to-one mapping between  $Z_e$  and  $\sigma_c(\cdot)$  that allows estimating for  $Z_e$  from the observed projection data.

### Monochromatic SIRZ Decomposition

The Monochromatic SIRZ method described in [4] shows that if we were to collect the projection data with two monochromatic X-ray sources at photon energies  $E_1$  and  $E_2$ ; and then construct two different attenuation images, one for  $\mu_1(E_1)$ , which is the attenuation coefficient at  $E_1$ , and the other for  $\mu_2(E_2)$ , the attenuation coefficient at  $E_2$ ; we could then use the logic of the previous section to characterize the voxels with  $(\rho_e, Z_e)$  values.

Since the basic SIRZ method, as described in the previous section, models X-ray attenuation as  $\mu(E) = \rho_e \cdot \sigma_c(Z, E)$ , a monochromatic approximation makes the dual-energy decomposition in the image space straightforward for the method described in [4]. This method first converts the decomposed DE sinograms (i.e., the Compton and PE line integrals) into “synthesized monochromatic” versions via the following linear transformation:

$$\begin{bmatrix} \bar{\mu}_1 \\ \bar{\mu}_2 \end{bmatrix} = \begin{bmatrix} f_{KN}(\hat{E}_1) & f_p(\hat{E}_1) \\ f_{KN}(\hat{E}_2) & f_p(\hat{E}_2) \end{bmatrix} \begin{bmatrix} A_c \\ A_p \end{bmatrix} \quad (12)$$

where  $\hat{E}_1$  and  $\hat{E}_2$  are generally taken as the mean photon energies in the two spectra while the terms  $A_c$ ,  $A_p$ ,  $f_{KN}(E)$ ,  $f_p(E)$  have been defined previously in Eqs. (2) and (3). Note that the Compton-PE bases can be replaced by any equivalent material basis functions for DE decomposition. The images reconstructed from the transformed line integrals are then decomposed into the  $(\rho_e, Z_e)$  images by simply solving the following equations for each voxel  $(a_{\hat{E}_1}, a_{\hat{E}_2})$ :

$$\begin{aligned} a_{\hat{E}_1} &= \rho_e \cdot \sigma_c(\hat{E}_1, Z_e) \\ a_{\hat{E}_2} &= \rho_e \cdot \sigma_c(\hat{E}_2, Z_e) \end{aligned} \quad (13)$$

Using mean spectral energies in Eq. (12) does not always completely compensate for the polychromatic nature of spectra — because two different X-ray spectra can have very similar mean spectral energies. As a result, [4] employs correction strategies to find the best monochromatic energy levels for the transformation in Eq. (12). This is only a brief description of the method proposed in [4]; the interested reader is advised to refer to the paper for a detailed understanding.

### The Proposed Method – AdaSIRZ

In this section, we propose the adaptive SIRZ (AdaSIRZ) decomposition method that extends the Monochromatic SIRZ method to the entire X-ray spectrum of the DECT source. By parameterizing X-ray attenuation directly over the cross-section surface in Figure 2, the method effectively bypasses the theoretical upper limit on  $Z_e$  estimation.

### AdaSIRZ Decomposition

First note that the SIRZ parameter space  $(\rho_e, Z_e)$  is more complex than the  $(a_c, a_p)$  parameters space used for the CPB method. Unlike the linear model shown in Eq. (2), SIRZ does not involve a linear combination of  $\rho_e$  and  $Z_e$ . Also, unlike the

Compton-PE basis functions that are continuous and monotonically decreasing curves, the X-ray cross-section curve  $\sigma(E)$  for a given  $Z$  is riddled with discontinuities from absorption edges, as shown in Figure 2. As a result, the optimization cost function for the decomposition involved will have a set of distinct local minima, one within each of the sub-regions shown in Figure 2.

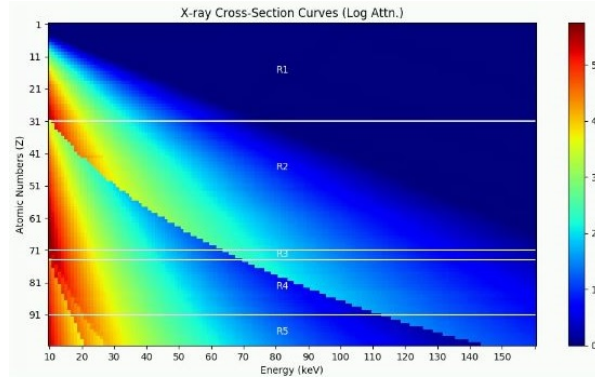


**Figure 2.** X-ray cross-section curves for natural elements with  $Z = 1$  to 100: The cross-section curve are plotted for the natural elements for the energy range of 10 keV to 160 keV. Through the linear interpolation in Eq. (10), the plot shown becomes a surface on which  $Z_e, E$  can be distinctly mapped. Using the number of discontinuities as a criterion, this surface can be divided into the subregions R1 through R5 as shown in the figure.

The AdaSIRZ decomposition method is executed for a pair of DECT attenuation coefficient values by solving the following constrained optimization problem:

$$\begin{aligned} Z_e^*, \rho_e^* &= \underset{Z_e, \rho_e}{\operatorname{argmin}} \sum_{i \in \{1,2\}} \left[ -\ln \int S_i(E) e^{-\rho_e \cdot \sigma_c(Z_e, E)} dE - \mu_i \right]^2 \\ &\text{subject to } Z_e \geq 1, \rho_e > 0 \end{aligned} \quad (14)$$

where  $\mu_1, \mu_2$  are the pixel values obtained from image reconstructions of the DECT projection data. We make use of the DogLeg method [14] for implementing the bounded optimization in Eq. (14). For convergence in each subregion in Figure 2, we initialize  $Z_e$  with the atomic number of a natural element whose true cross-section response for the given DE spectra is closest to the observed values for  $\mu_1$  and  $\mu_2$ . That is,

$$Z_e^{(0)} = \underset{Z}{\operatorname{argmin}} \left\| - \begin{bmatrix} \ln \sum_E S_1(E) e^{-\rho_e \cdot \sigma_Z(E)} \\ \ln \sum_E S_2(E) e^{-\rho_e \cdot \sigma_Z(E)} \end{bmatrix} - \begin{bmatrix} \mu_1 \\ \mu_2 \end{bmatrix} \right\| \quad (15)$$

where  $S_1(E), S_2(E)$  are the discretized DE spectra while  $\sigma_Z(E)$  and  $\rho_{e,Z}$  are the X-ray cross-section and standard electron density of the natural element  $Z$ , respectively. This is what we refer to as *forced initialization* for AdaSIRZ. The opposite case would be a *fixed initialization*, i.e., initializing with a fixed value for  $Z_e^{(0)}$  for all cases.

As shown in the next section, an optimization with the above initialization provides for better  $Z_e$  approximation than with a fixed initial value. That is because approximating the traversed element in a voxel taking into account the estimated attenuation  $\mu_1, \mu_2$  improves the chances that the initialization as shown above

would land in the correct subregion for the cross-sections shown in Figure 2. We confirm this with the evaluation of AdaSIRZ decomposition on real and simulated images in the next section.

## Results

### Experimental Setup

To analyze the performance of AdaSIRZ decomposition, we have tested the method on a set of real and simulated Dual Energy CT projections and compared its output with those obtained with CPB and with Monochromatic SIRZ (MonoSIRZ).

All computations were carried out on a cloud cluster computing node VM with 16 CPU cores, 32 GB RAM and a single GPU for parallel-processing. Unless otherwise noted, the DECT energy spectra were modeled after the X-ray sources used in the Imatron C300 scanner for 95 kVp and 130 kVp peak voltages respectively for both the simulation projections and the real projections from the ALERT TO-3 dataset [5]. The cross-section curves for the natural elements were obtained from the NIST XCOM Database [15] for both the CT simulation and for implementing the cross-section surface in Figure 2 for AdaSIRZ optimization.

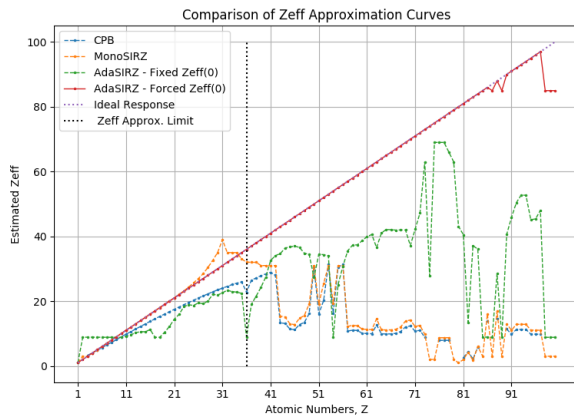


**Figure 3.**  $Z_e$  approximation curves: The plot shows the  $Z_e$  estimates for the following four methods: (i) CPB decomposition; (ii) Monochromatic SIRZ (MonoSIRZ); (iii) AdaSIRZ with a fixed initialization for  $Z_{eff}^{(0)}$ ; and (iv) AdaSIRZ with a forced initialization for  $Z_{eff}^{(0)}$  as described in Eq. (15).

### $Z_e$ Approximation Curves

To determine the theoretical operating limits of the proposed method, we plotted the  $Z_e$  approximation curves for the three methods using the same methodology used for the results shown in Figure 1. To calculate the  $Z_e$  values, forward projection value pairs were calculated for the DE spectra for ray traversal through a unit volume of each of the natural elements. The calculated attenuation values were then decomposed using the three methods to obtain the estimated  $Z_e$ . From the resulting plots, we see that the performance of CPB and MonoSIRZ is limited by the theoretical upper limit ( $Z = 35$  for the 95 keV and 130 keV spectra) while AdaSIRZ is not. Also, AdaSIRZ has a theoretical approximation response that is very close to the ideal response for the entire range. That is because the method models directly after the X-ray cross sections [15] which in the absence of noise uniquely correlates with the natural element. We also see the difference in performance for two different initializations for AdaSIRZ.

## Simulation Results

A pair of Dual Energy CT projections ( $360 \text{ views} \times 256 \text{ channels}$ ) were simulated with a projection geometry modeled after the Imatron C300 scanner and using the 95 keV and 130 keV X-ray spectra [5]. The reconstructed DECT images shown in Figure 4 consist of a cylindrical water body containing eight constituent material cylinders: graphite, pyrex, neoprene, Al, Ti, Fe, Cu, and Sn.  $Z_e$  images were estimated for the reconstructions using the three methods which are illustrated in Figure 4 (a). The statistical results are also enumerated in Table 1.

**Table 1: Results on Simulated Images**

	GT	CPB	MonoSIRZ	AdaSIRZ
C	6	$7.02 \pm 2.71$	$5.93 \pm 3.75$	<b><math>5.96 \pm 3.47</math></b>
G <sup>1</sup>	10.7	<b><math>10.94 \pm 1.42</math></b>	<b><math>10.29 \pm 1.40</math></b>	<b><math>10.32 \pm 3.55</math></b>
R <sup>2</sup>	11.4	$12.14 \pm 5.10$	<b><math>11.18 \pm 3.30</math></b>	$10.90 \pm 5.85$
Al	13	$12.82 \pm 1.55$	$13.61 \pm 2.31$	<b><math>13.04 \pm 3.67</math></b>
Ti	22	$19.60 \pm 1.41$	$21.12 \pm 2.44$	<b><math>21.19 \pm 1.08</math></b>
Fe	26	$20.22 \pm 7.89$	$22.94 \pm 9.27$	<b><math>25.14 \pm 1.69</math></b>
Cu	29	$9.14 \pm 0.23$	$3.00 \pm 0.00$	<b><math>29.89 \pm 1.64</math></b>
Sn	50	$8.30 \pm 0.00$	$3.00 \pm 0.00$	<b><math>54.81 \pm 0.00</math></b>

<sup>1</sup>G - Glass (Pyrex) -  $Z_e$  for pyrex varies between 10.07-11.0.

<sup>2</sup>R - Neoprene.

**Table 2: Results on ALERT TO-3 Dataset**

	GT	CPB	MonoSIRZ	AdaSIRZ
H <sub>2</sub> O	7.4	$6.79 \pm 2.83$	$7.11 \pm 2.64$	<b><math>7.34 \pm 2.56</math></b>
Mg	12	$11.17 \pm 0.37$	<b><math>12.68 \pm 0.44</math></b>	<b><math>12.68 \pm 0.43</math></b>
Si	14	$13.14 \pm 1.87$	$13.21 \pm 3.23$	<b><math>14.35 \pm 2.21</math></b>
C	6	$6.88 \pm 0.93$	$7.12 \pm 1.10$	<b><math>6.14 \pm 1.01</math></b>

### Results on ALERT TO-3 Dataset

The performance of AdaSIRZ was further tested on a set of real Dual Energy CT projections ( $720 \text{ views} \times 512 \text{ channels}$ ) obtained from the ALERT TO-3 dataset [5]. The images consist of scans of a number of reference materials using the setup described before. The results for the  $Z_e$  images reconstructed using the three methods are shown in Figure 4 (b)-(c) while the reconstruction statistics for the materials are enumerated in Table 2.

From the numerical results presented in Tables 1 and 2, we see that  $Z_e$  estimation obtained with AdaSIRZ performs well on both the simulated and the real images from the ALERT dataset. While AdaSIRZ in general suffers from a higher variance, its operating range for  $Z_e$  far exceeds that of CPB or MonoSIRZ as is evident in Table 1. Since the proposed method focuses only on atomic number estimation, we are not in a position to make any comments regarding the density characterization of the proposed decomposition.

## Conclusion

We have proposed a new extension of the SIRZ algorithm that can be used for a wider range of materials for practical scanner setups. The formal analysis of the limits of Compton-PE basis decomposition puts into sharper focus the need for flexible meth-

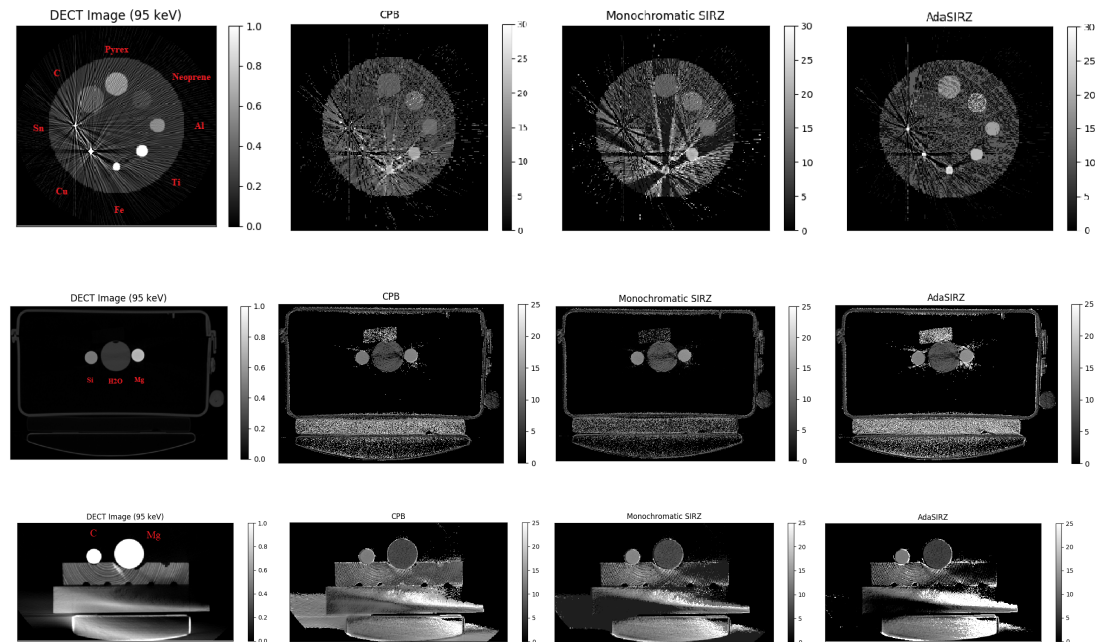


**Figure 4.** Results for  $Z_e$  estimation on real and simulated images: The images show atomic number reconstructions using each of the three methods: CPB, MonoSIRZ, and AdaSIRZ and for three different images. The three images include (a) Simulated DECT Image with nine constituent materials, (b) DECT Image from ALERT TO-3 Dataset: Reference Materials -  $H_2O$ , Si, Mg) and (c) DECT Image from ALERT TO-3 Dataset: Reference Materials - C, Mg. The statistics for the labeled materials in the images are provided in Tables 1 and 2.

ods for  $Z_e$  estimation. With robust strategies for initialization, the AdaSIRZ method can lend itself to meeting these needs for material characterization.

## References

- [1] R. Murty, Effective atomic numbers of heterogeneous materials, *Nature* **207**(4995) (1965), 398.
- [2] Z. Ying, R. Naidu and C.R. Crawford, Dual energy computed tomography for explosive detection, *Journal of X-ray Science and Technology* **14**(4) (2006), 235–256.
- [3] S.G. Azevedo, H.E. Martz, M.B. Aufderheide, W.D. Brown, K.M. Champley, J.S. Kallman, G.P. Roberson, D. Schneberk, I.M. Seetho and J.A. Smith, System-independent characterization of materials using dual-energy computed tomography, *IEEE Transactions on Nuclear Science* **63**(1) (2016), 341–350.
- [4] K.M. Champley, S.G. Azevedo, I.M. Seetho, S.M. Glenn, L.D. McMichael, J.A. Smith, J.S. Kallman, W.D. Brown and H.E. Martz, Method to Extract System-Independent Material Properties From Dual-Energy X-Ray CT, *IEEE Transactions on Nuclear Science* **66**(3) (2019), 674–686.
- [5] *Final Report - ALERT TO-3 Reconstruction Initiative*, [https://myfiles.neu.edu/groups/ALERT/strategic\\_studies/TO3\\_FinalReport.pdf](https://myfiles.neu.edu/groups/ALERT/strategic_studies/TO3_FinalReport.pdf), Boston, Massachusetts, 2013.
- [6] R.E. Alvarez and A. Macovski, Energy-selective reconstructions in x-ray computerised tomography, *Physics in Medicine & Biology* **21**(5) (1976), 733.
- [7] E.M. Hussein and E.J. Waller, Review of one-side approaches to radiographic imaging for detection of explosives and narcotics, *Radiation Measurements* **29**(6) (1998), 581–591.
- [8] G. Harding, X-ray scatter tomography for explosives detection, *Radiation Physics and Chemistry* **71**(3–4) (2004), 869–881.
- [9] F. Li, A. Manerikar, T. Prakash and A. Kak, A Splitting-Based Iterative Algorithm for GPU-Accelerated Statistical Dual-Energy X-Ray CT Reconstruction, *arXiv preprint arXiv:1905.00934* (2019).
- [10] R. Zhang, J.-B. Thibault, C.A. Bouman, K.D. Sauer and J. Hsieh, Model-based iterative reconstruction for dual-energy X-ray CT using a joint quadratic likelihood model, *IEEE transactions on medical imaging* **33**(1) (2014), 117–134.
- [11] G. Landry, J. Seco, M. Gaudreault and F. Verhaegen, Deriving effective atomic numbers from DECT based on a parameterization of the ratio of high and low linear attenuation coefficients, *Physics in Medicine & Biology* **58**(19) (2013), 6851.
- [12] W. Mayneord, The significance of the roentgen, *Acta Int Union Against Cancer* **2** (1937), 271.
- [13] E. Merritt, X-ray Absorption Edges, <http://skuld.bmsc.washington.edu/scatter/AS-periodic.html>, 2010.
- [14] C. Voglis and I. Lagaris, A rectangular trust region dogleg approach for unconstrained and bound constrained nonlinear optimization, in: *WSEAS Int. Conf. Appl. Math.*, 2004.
- [15] M.J. Berger and J. Hubbell, XCOM: Photon cross sections on a personal computer, Technical Report, National Bureau of Standards, Washington, DC (USA). Center for Radiation Research, 1987.

## Author Biography

Ankit Manerikar received his B.E. degree in Electronics Engineering with distinction from Mumbai University (2015) and his M.S. degree in Electrical & Computer Engineering from Purdue University (2017). His key research interests include X-ray image processing, machine learning for CT segmentation and automatic target detection. He is currently a PhD student at Robot Vision Lab, Purdue University with a research focus on Computer Vision and has authored several publications in this area.

**JOIN US AT THE NEXT EI!**

IS&T International Symposium on

# Electronic Imaging

SCIENCE AND TECHNOLOGY

*Imaging across applications . . . Where industry and academia meet!*



- **SHORT COURSES • EXHIBITS • DEMONSTRATION SESSION • PLENARY TALKS •**
- **INTERACTIVE PAPER SESSION • SPECIAL EVENTS • TECHNICAL SESSIONS •**

[www.electronicimaging.org](http://www.electronicimaging.org)

